OXFORD

Journal of Geophysics and Engineering

Journal of Geophysics and Engineering (2020) **17**, 439–450 doi:10.1093/jge/gxaa003

High-resolution inversion for dispersion characteristics of acoustic logging waveforms

Da Chen[1], **Wei Guan**[1,*], **Chao Zhang**[1], **Qihang Zhou**[2] **and Hengshan Hu**[1]

[1] Department of Astronautics and Mechanics, Harbin Institute of Technology, Harbin 150001, China
[2] Beijing Institute of Astronautical Systems Engineering, Beijing 100000, China

*Corresponding author: Wei Guan. E-mail: guanw@hit.edu.cn

Received 4 May 2019, revised 8 January 2020
Accepted for publication 15 January 2020

Abstract

In acoustic logging, most published studies of extracting array data characteristics are difficult to avoid the interference from the false modes. The false modes contribute little to the acoustic waveforms but makes the true modes hard to identify. We introduce a threshold of the energy spectrum into the pole-calculation method to remove the false modes, thereby eliminating their interferences to the true modes. To avoid the separation of multiple crossings of pole distribution, we directly acquire the slowness dispersion of multiple modes by superposing the single-mode results calculated from the weighted spectral semblance method. We processed the slowness-frequency snapshot and design an extreme-point extraction formula to generate the multi-mode scatterplot, which provide a precise slowness dispersion result. In terms of four synthetic cases of acoustic logging, it has demonstrated that the proposed algorithm can provide a high-resolution slowness dispersion profile for multiple modes. Even for acoustic logging while drilling with strong tool wave components, the aliases and interferences of false modes do not exist. Finally, a test proves that the proposed algorithm also has a good anti-noise ability.

Keywords: acoustic logging, mode-wave extraction, slowness dispersion, matrix pencil, weighted spectral semblance

1. Introduction

In acoustic logging for oil-gas exploration, the full waveforms in the time domain recorded in the borehole are composed of various wave groups, normally including the compressional (P-) wave, the shear (S-) wave, the Stoneley (St) wave, the Pseudo-Rayleigh (PR) wave and others. Some of them are obviously dispersive, especially mode waves such as the PR wave. Dispersion characteristics of these mode waves have a close relationship with the lithological and mechanical behaviors of formations, which is helpful when analysing formation anisotropy (Sinha *et al.* 1994; Xu *et al.* 2017), acquire formation P- and S- wave slowness (Tang *et al.* 1995; Jiang *et al.* 2017) and estimate formation stress (Sinha *et al.* 2000; Plona *et al.* 2002).

Many attempts have been made to obtain the dispersion characteristics of different wave groups accurately. Various methods of dispersion analysis generally fall into two categories until now: single-mode analysis and multimode analysis. As a kind of method for single-mode analysis, the phase unwrapping algorithm has been proposed by Tribolet (1977) for seismic signal processing, and was then extended by Su & Qiao (2003) to extract phase velocity of dispersive wave. Another widely-used method for single-mode analysis is weighted spectral semblance (Nolte *et al.* 1997), which inverts the true modes by searching the maximum of the semblance function within a certain slowness range and then rejecting the meaningless null solution (Tang & Cheng 2004). The weighted spectral semblance (WSS) algorithm is stable and efficient, which has been applied to the cross-dipole acoustic logs successfully (Sinha *et al.* 2000). However, these single-mode methods can only

extract the strongest mode, which is inapplicable for complex signals involving multiple mode waves. By contrast, multimode analysis extracts all the mode waves simultaneously at a given frequency, such as the Prony algorithm (Lang *et al.* 1987; Tang 1997), matrix pencil algorithm (Hua & Sarkar 1990; Ekstrom 1996) and amplitude and phase estimation algorithm (Li & Stoica 1996). Conventional methods for multimode analysis, without exception, bring about periodic aliases when calculating the slowness, which reduces the resolution of dispersion graphs seriously. To resolve this issue, Tang & Cheng (2004) and Ma *et al.* (2010) combine Prony algorithm with WSS, Wang *et al.* (2012) mesh matrix pencil algorithm with WSS, and also applied a pole calibration scheme to distinguish different individual mode. Li *et al.* (2015) extend the amplitude and phase estimation (APES) algorithm to forward and backward amplitude and phase estimation (FBAPES) algorithm. Recently, Zeng *et al.* (2018) combine the semblance of slowness-time coherence based on differential phase (STC-DP) processing with band pass filtering algorithm. Although these combined or modified algorithms have significantly improved the inversion results of the slowness dispersion, a performance-affected issue caused by false modes still need to be addressed. Because the number of true modes is uncertain and varies with frequency, a setting number greater than that of the true modes is required for almost all the multimode algorithms. This produces some false modes interfering with the true modes in the dispersion graph.

In order to avoid the interference caused by false modes and thereby improve the accuracy and resolution of the inversion, we adopt a filtered strategy in this study according to the characteristic of frequency-spectrum energy to remove the false modes. In this case, we only need to calculate the true modes instead of solving all (the number has been preset) the modes together as in previous studies. Besides, without using the pole calibration scheme (Wang *et al.* 2012) to distinguish different modes, we directly superimpose the discontinuous slowness results of individual modes to obtain a slowness graph containing complete dispersion of the true modes. In addition, we present the extreme-point extraction scheme to improve the resolution. The final result is shown in the form of scatterplot rather than slowness-frequency snapshot. In the rest of this paper, we first detail the four steps of the proposed algorithm. Then we check the algorithm in terms of four synthetic cases, including the acoustic logging while drilling (LWD) that has complex wave components. Furthermore, we tested the algorithm's anti-noise ability in the case of LWD. By comparison of the results between different algorithms, we demonstrate the advantage of the proposed algorithm. Finally, we summarise the innovation points and conclusions.

2. Methodology

The algorithm proposed in this study consists of the following four segments: (1) calculating the poles of the mode waves by matrix pencil (MP) algorithm; (2) removing the false modes according to a two-step scheme: sort all the modes by the absolute value of complex amplitude first and then eliminate the false modes; (3) inverting the dispersion slowness of the true modes by WSS and eliminating the aliases; and (4) extracting the extremum and generating the slowness-frequency scatterplot.

2.1. Matrix pencil (MP) algorithm

In the first step to extract the dispersion information of acoustic logs, the received array acoustic signals should be Fourier-transformed from time domain to frequency domain. According to the theory of borehole acoustics, the frequency spectrum $X(z_n, \omega)$ can be approximately expressed as the sum of various mode waves,

$$X(z_n, \omega) \approx \sum_{l=1}^{p} a_l(\omega)\, e^{ik_l(\omega) z_n},\ (n = 0, 1 \ldots, m-1), \tag{1}$$

where z_n is the distance from the source to the $(n+1)$-th receiver, ω is the angular frequency, p is the number of the mode waves existing in the frequency spectrum (it is a hypothesis value), m is the number of receivers a_l and k_l are the amplitude and wavenumber of the l-th mode wave, respectively. At a given frequency ω_0, we abbreviate $X(z_n, \omega_0)$ to $x(n)$ for simplicity. Then substitute $z_n = z_0 + n\Delta z$ and two complex variables $b_l = a_l\, e^{ik_l z_0}$ and $\lambda_l = e^{ik_l \Delta z}$ into equation (1), which yields

$$x(n) \approx \sum_{l=1}^{p} b_l \lambda_l^n,\ (n = 0, 1 \ldots, m-1), \tag{2}$$

where Δz is the distance between adjacent receivers. The value p is set according to the number of true modes and should meet $q \le p \le m - q$ (Ekstrom 1996), where q is the number of true modes. Since q is uncertain, a setting number p greater than q is required. Normally, $p = \frac{m}{2}$ is appropriate, and we adopt this principle in this paper $(m = 13)$.

The MP algorithm, proposed by Hua & Sarkar (1990) and then improved by Ekstrom (1996), can be used to invert the poles λ_l ($l = 1, 2 \ \ldots \ , p$) when the inter-space between receivers is appropriate and the number of mode waves is less than the number of receivers ($p < m$). Ekstrom (1996) explains the decomposition principle and steps of MP algorithm in detail. By constructing a parent Hankel matrix (X) and two submatrices ($X0$ and $X1$) according to $x(n)$, the inversion problem of λ_l changes to the eigenvalue calculation of $([X1]^{+}[X0] - \lambda[I])e = 0$, and this is called forward MP calculation, where the superscript '+' denotes the operation of Moore–Penrose generalised inverse (Penrose 1955). Likewise, the poles λ_l can also be obtained by calculating the eigenvalue of $([X0]^{+}[X1] - \lambda[I])e = 0$ with the flip sequence of observed data, and this is called backward MP calculation. From the forward and backward MP calculations, we can obtain two results, λ_l^f and λ_l^b, respectively. If their phase difference is less than the specified tolerance (Ekstrom 1996), the calculated pole is identified as the right one (the final result is averaged by $\lambda_l = \sqrt{\lambda_l^f \cdot \lambda_l^b}$), or else it is considered as noise signal.

2.2. *Removal of false modes*

Once the poles λ_l are obtained, we can use the least square method to calculate the complex amplitudes b_l corresponding to the p mode waves (Wang *et al.* 2012). By this means, the spectrum of the full waveform is decomposed into multiple ones for the p mode waves. As a result, the problem changes from multimode analysis to single-mode analysis.

Among these p mode waves, we are interested in the true ones that have larger amplitude; they are the major contributors to the acoustic logging waveforms. Nevertheless, the number of these true modes is uncertain and varies with frequency because some of them tend to cut off at low frequencies and attenuate at high frequencies. Since the number of true modes cannot be determined, people tend to set a value p that is greater than the number of true modes and then invert the p setting modes. As a result, it is probable to calculate some mode waves with small amplitude (called false modes), which have negligible contributions to the full waveforms but result in significant interference to the true modes. For this case, we propose a two-step scheme to eliminate such influence of these false modes and improve the resolution of dispersion graph.

First, we sort the p mode waves in terms of their amplitudes ($l = 1, 2 \ \ldots \ , p$). Since the amplitude spectrums of different modes are almost the same on all receivers, p modes can be sorted on any receivers (such as the first one).

$$\mathbf{B}' = \begin{bmatrix} b_1'(z_0, \omega_1) & b_1'(z_0, \omega_2) & \ldots. & b_1'(z_0, \omega_N) \\ b_2'(z_0, \omega_1) & b_2'(z_0, \omega_2) & \ldots. & b_2'(z_0, \omega_N) \\ \ldots. & \ldots. & \ldots. & \ldots. \\ \ldots & \ldots. & \ldots. & \ldots. \\ b_p'(z_0, \omega_1) & b_p'(z_0, \omega_2) & \ldots. & b_p'(z_0, \omega_N) \end{bmatrix}, \tag{3}$$

where $\mathbf{B}'$ is the sorted spectrum matrix; $\omega_i (i = 1, 2, \ \ldots \ N)$ is frequency sampling point $b_i'(i = 1, 2, \ \ldots \ P)$ is the amplitude of the sorted mode arranged in descending order (b_1' is maximum, b_p' is minimum).

Then we calculate the energy defined as follows according to Parseval theorem (Tamarkin 1926),

$$E_l = \sum_{j=1}^{N} \left| b_l'\left(z_0, \omega_j\right) \right|^2, \quad l = 1, 2, \cdots, P, \tag{4}$$

where E_l reflects the contribution of the l-th row of the matrix $\mathbf{B}'$ to the full waveforms. It is found that the difference of E_l between different rows is significant (several orders of magnitude). Therefore, we introduce a threshold and propose equation (5) to distinguish the true modes dominating the full waveform from all the modes,

$$\left\{ \begin{array}{ll} E_l \geq \beta\% * E_{l(max),} & \text{Retain} \\ E_l < \beta\% * E_{l(max),} & \text{Remove} \end{array} \right\}, l = 1, 2, \cdots, P, \tag{5}$$

where β is the threshold coefficient. If the energy value of one mode is less than $\beta\%$ of the maximum value ($E_{l(\max)}$), this mode is considered as the one with negligible contribution or the false mode and thus needs to be removed. Conversely, this mode is considered as the one dominating the full waveform and thus needs to be retained. The value of β is dependent on the value of E_l. Similar to the means of choosing the effective value in singular value decomposition, we determine the threshold

coefficient β by finding sudden changing point of the E_l value (Zhao & Ye 2011). In our study, we set $\beta = 0.01$ that performs well for all the following cases.

Following the steps mentioned above, we can determine the number of the dominant modes and remove the false modes, by which the interference from the false modes will be eliminated in final slowness dispersion graph.

2.3. *Calculation of slowness dispersion without aliases*

As a high-performance method for single-mode analysis, WSS (Nolte *et al.* 1997) is modified in this study for the issue of slowness dispersion of signals with multiple mode waves. By calculating the self-correlation coefficients of all the predetermined slowness-frequency points, we can obtain a series of slowness-frequency snapshots representing each single-mode. Note that the so-called single-mode snapshot is not a pure one that could perfectly display the dispersion characteristic of a single mode wave, but involves two or more modes. Actually, the dispersion profiles in these snapshots are generally discontinuous in different frequency range. This is because not all the matrix elements in each row of equation (3) belong to the same mode. To solve this problem, Wang *et al.* (2012) attempted to adopt the means of pole calibration to separate different modes. Although their method works well for the cases involving a small number of modes, it is difficult to obtain a pure single mode when there are many modes with multiple crossings of pole distribution. Consequently, we put to an alternative to construct the slowness dispersion for the multiple mode waves by directly superimposing all the single-mode results calculated by WSS. It is unnecessary to pursue a pure single mode before the WSS calculation. Although the dispersion profiles of each single mode calculated by WSS is still discontinuous, the superimposition of them is indeed complete and continuous. This also indicates that the true modes are not filtered out in the process of removing the false modes by the means of subsection 2.2, otherwise we cannot obtain the complete result of full-mode from the superposition of disorganised single-mode results.

The premise of applying WSS is to choose an appropriate slowness range. It should be noted that the phase ambiguity of $\lambda_l = e^{is_l\omega\Delta z}$ will lead to that the slowness s_l is periodically multi-valued with the period of $\frac{2\pi}{\omega\Delta z}$, which brings a barrier of choosing slowness range when applying WSS. To determine the correct range of the slowness, we employ the scheme given in previous studies (Ma *et al.* 2010; Wang *et al.* 2012). Firstly, we need to determine an approximate slowness s_c, which is determined by the time-slowness coherence (STC) method (Kimball & Marzetta 1984), then we consider the correct phase of all the modes should be changed in the neighborhood of 2π centered on $s_c\omega\Delta z$, that is

$$s_c\omega\Delta z - \pi < s\omega\Delta z < s_c\omega\Delta z + \pi. \tag{6}$$

To sum up, the semblance coefficients of each mode can be calculated according to

$$\left\{\begin{array}{ll} \rho_l(\omega,s) = \dfrac{\left|\sum_{n=0}^{m-1} b_l'^{*}(z_n,\omega)\exp(-nis\omega\Delta z)\right|}{\sqrt{(m-1)\sum_{n=0}^{m-1} b_l'^{*}(z_n,\omega)b_l'(z_n,\omega)}}, & s_c - \dfrac{\pi}{\omega\Delta z} < s < s_c + \dfrac{\pi}{\omega\Delta z} \\ \rho_l(\omega,s) = 0 & \text{else} \end{array}\right\}, \tag{7}$$

where $b_l'^{*}$ is complex conjugate of b_l'; s represents each value in the selected slowness range. Equation (7) means if the selected slowness is within the limited range, then calculate the semblance coefficient; if not, consider it as aliases and set the semblance coefficient to zero. In addition, to improve the smoothness of the result, we suggest adopting the weighted method using nearby frequency points for every assigned frequency (Ma *et al.* 2010).

Finally, the weighted semblance coefficients of P' single modes are superimposed at the corresponding slowness-frequency locations. In this way, we obtain the full-wave slowness-frequency semblance coefficients $F(\omega, s)$ as

$$F(\omega,s) = \sum_{l=1}^{p'} \rho_l(\omega,s). \tag{8}$$

2.4. *Acquisition of slowness-frequency scatterplot*

Most previous studies use slowness-frequency snapshots to analyse the mode wave dispersion. Comparing with low-resolution snapshots, we provide scatterplots with higher resolution, which are generated automatically by using code. The scatterplots are acquired by extracting the extremum of the semblance coefficient at different frequencies. It is important to note that these extremum points are not extracted directly from the superposed dispersion graph containing all the modes, but from the single-mode dispersion slowness-frequency snapshot, respectively. The reason is that single-mode has the property of slowness-frequency one-to-one correspondence. It means for a single-mode slowness graph each frequency point only

corresponds to one slowness value. When for the full-mode slowness graph, because some modes have cut-off frequencies, the number of slowness extremum may change when in different frequency. This will lead to difficulty in determining the number of extremums. Therefore, we adopt a scheme to acquire the final slowness scatterplot of full-mode by superimposing the extremum of each single mode extracted.

The extreme-point extraction scheme is specified as follows including two steps. First, we optimise the slowness-frequency snapshot of each mode by setting the values with smaller semblance coefficients to zero. The reason being some modes have cut-off frequencies. If the small values are not set to zero, the extremums outside the cut-off frequency will appear when applying extreme-point extraction scheme. Obviously, these values are incorrect and can be removed by optimisation means as

$$\left\{\begin{array}{ll} F'(\omega,s)=F(\omega,s) & F(\omega,s)\geq\alpha*F_{max}(\omega,s) \\ F'(\omega,s)=0 & \text{else} \end{array}\right\}, \tag{9}$$

where α is the optimised coefficient, it performs well in practice when α is set between 0.5 and 0.8. Note that if α is too large, some real mode information will be filtered out. $F_{max}(\omega,\ s)$ is the maximum value in the semblance coefficient matrix. $F'(\omega,\ s)$ represents the coefficient after optimising.

The second step is to extract the extremum of the semblance coefficients of each single mode and then superimpose them, by which we obtained extremum matrix $\mathbf{Z}$ containing all the true modes as

$$\mathbf{Z}=\sum_{l=1}^{p'}\left[Z_l(F_l)\right]\Big|_{F_l=\max\limits_{k=1}^{N}(F_l(\omega_k,s))}, \tag{10}$$

where N is the number of the discrete frequency points and $Z_l(F_l)$ is the corresponding slowness-frequency coordinate of the l-th mode. Equation (10) means that for the l-th mode, the locations of the maximum value of the coefficient $F_l(\omega_k,\ s)$ are selected at each frequency point ω_k. Then we superimpose the coordinate locations of these P' modes. Finally, we can obtain the slowness dispersion scatterplot according to $\mathbf{Z}$.

2.5. *Processing flow chart*

To sum up, the modified MP algorithm we proposed consists of four steps. Besides, we provide two forms of dispersion result. The processing flow chart is as follows:

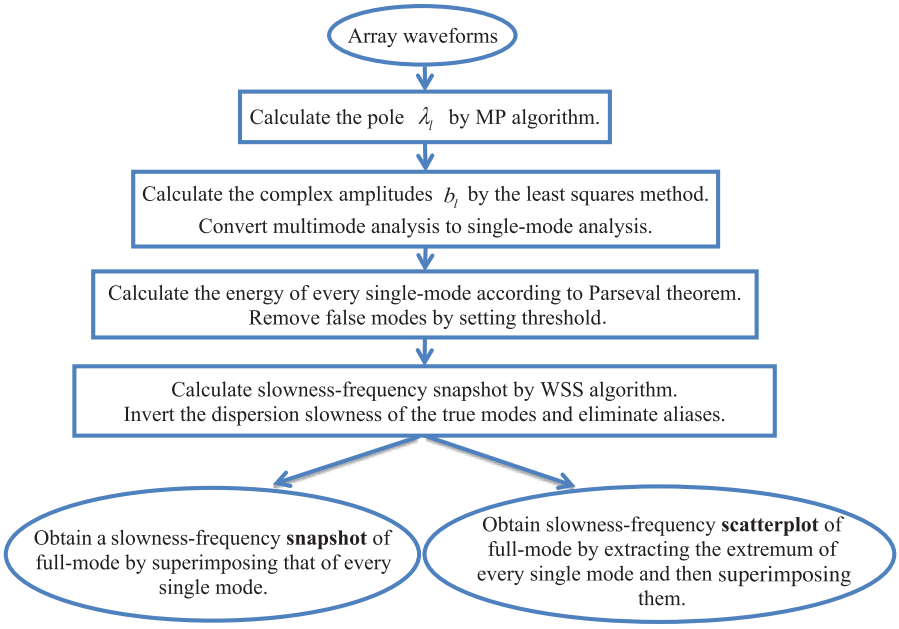

Table 1. Properties of the borehole fluid and formations.

	Hard formation	Soft formation	Drill collar	Borehole fluid
V_P (m s^{-1})	3970	2000	5860	1470
V_S (m s^{-1})	2455	1000	3130	—
ρ (kg m^{-3})	2320	2000	7800	1000

3. Numerical examples

In this section, we check the aforementioned mode-wave inversion algorithm in terms of four different cases, including the monopole acoustic logging in a hard formation and the dipole acoustic logging in a hard formation and soft formation, respectively, as well as acoustic logging while drilling (LWD) in a hard formation. We apply the real-axis integration (RAI) method (Tsang & Rader 1979) to calculate the time-domain waveforms to be used as the initial data for inversion. The formation and borehole-fluid parameters (Zheng *et al.* 2015; Wang *et al.* 2015) for the following cases are listed in Table 1. The acoustic transmitter is assumed to be a cosine envelope pulse as

$$s(t) = \begin{cases} \frac{1}{2}\left[1+\cos\frac{2\pi}{T_c}\left(t-\frac{T_c}{2}\right)\right]\cos 2\pi f_0\left(t-\frac{T_c}{2}\right), & 0 \le t \le T_c, \\ 0, & t<0 \text{ or } t>T_c, \end{cases} \tag{11}$$

where f_0 and T_c denote the center frequency and the pulse width of the source, respectively.

For cases with hard and soft formations, the central frequency of sources are 12.0 and 5 kHz, respectively. The sound source is located on the axis of the fluid-filled borehole (wireline logging) or on the outer surface of drill collar (LWD). The sonic tool consists of 13 receivers at an inter-receiver spacing of 0.1 m, and the first receiver is 3.0 m away from the source. For each receiver, we record the waveforms of the first 10 ms that have covered all the mode waves. The borehole radius is set to 0.1 and 0.117 m, respectively for the wireline logging and the acoustic LWD. The inner and outer radii of the drill collar in acoustic LWD are 0.027 and 0.090 m, respectively.

3.1. *Monopole acoustic logging*

Figure 1 presents the forward and inversion results for monopole acoustic logging in a hard formation. Shown in figure 1a are the full waveforms in the time domain, where the dominant wave groups include the P-wave, the S- wave and PR wave as well as the St wave in order of arrival time. Figure 1b–1f are the slowness-frequency graphs obtained by processing time-domain waveforms in different means.

For the inversion result in figure 1b, the pre-number of mode waves p is set to seven. Without using the scheme mentioned in subsection 2.2, all the seven modes are involved in figure 1b. By contrast, only four mode waves are retained in figure 1c, corresponding to the four dominant wave groups. However, the number of mode waves is still set to seven, among which three false modes have been removed in figure 1c. In comparison to figure 1b and 1c, the negative effects of the false modes and the advantage of the modes-removal scheme proposed in this study are obvious. Because of the false modes, the slowness-frequency profiles for the true mode waves in figure 1b have discontinuity points at some frequencies. Such interferences are eliminated in figure 1c and thus the interested mode waves including the St wave and the PR waves of each order as well as the P- and S-waves are clearer.

Figure 1d shows the slowness-frequency snapshot obtained by using the conventional WSS algorithm. It is seen that the St wave, the first-order PR wave and higher-order PR waves just appear within 0–8, 8–20 and after 20 kHz, respectively. This is because the conventional WSS can only identify one single mode in each frequency. In addition, it can be found from the upper and lower right corners of figure 1d that the slowness-frequency snapshot obtained directly by WSS algorithm contains aliases. When observing the slowness-frequency snapshot in figure 1b or c after removing the aliases, there is a clear distinction of color in the upper and lower right corner. This is because the semblance coefficient of the original locations in figure 1d has been changed to zero. This indicates that the scheme in subsection 2.3 can effectively eliminate aliases. Figure 1e is the slowness-frequency snapshot after optimising, where there are no aliases and interferences of false mode waves. Compared with figure 1c without optimising, the resolution in figure 1e improves significantly.

Shown in figure 1f are the scatterplots of slowness for three algorithms, including the WSS, the modified MP algorithm and the forward synthetic algorithm. The forward synthetic result is calculated by finding the zero points of the characteristic equation according to the boundary conditions (Tang & Cheng 2004). By comparison, the advantage of the algorithm proposed in this study over the conventional WSS algorithm is obvious. For the WSS algorithm, the slowness points of the

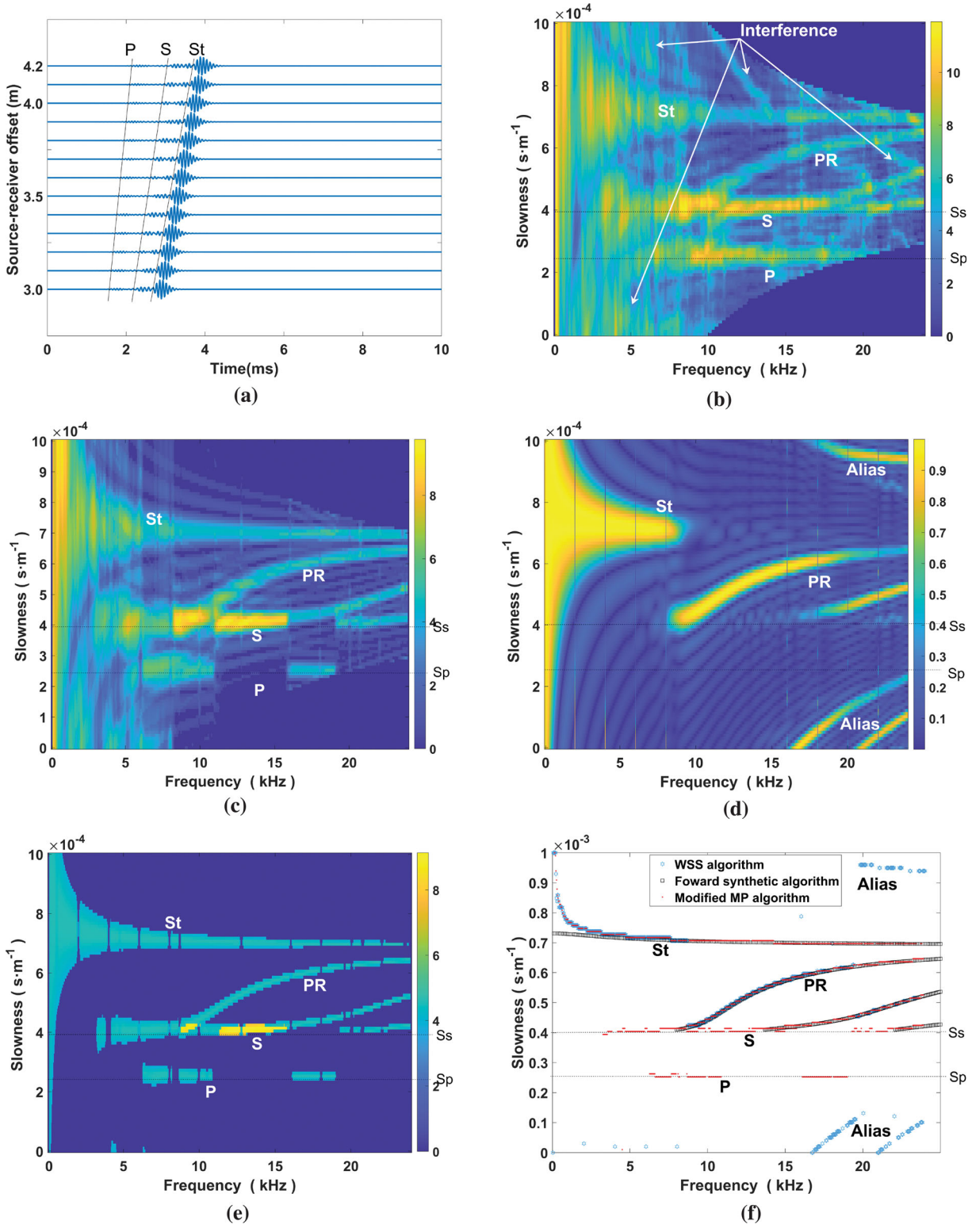

Figure 1. Monopole logging in the hard formation: (a) synthetic time-domain full waveforms; (b) slowness-frequency snapshot involved all the mode waves; (c) slowness-frequency snapshot with removing false modes; (d) slowness-frequency snapshot inverted by the WSS algorithm; (e) slowness-frequency snapshot inverted by the modified MP algorithm proposed in this study and (f) Comparison of dispersion scatterplot of WSS algorithm, modified MP algorithm and forward synthetic algorithm.

St wave and the first-order PR wave are displayed partially in the frequency domain, and those of the higher-order PR waves are hardly visible because of the aliases. For our algorithm, however, the slowness points of all the mode waves as well as the P- and S- waves are continuous and there are no aliases. Furthermore, by comparison with the result of forward synthesis algorithm (black square), the two kinds of scatterplot almost coincide, which also proves the correctness of modified MP algorithm proposed in this paper. Additionally, note that the extracted data of the St wave deviates from the forward result at extreme low frequencies, which is a small fault for all the mode-wave extraction algorithms. On the other hand, it can be found from comparison that the slowness resolution of the scatterplot in figure 1f is higher than that in figure 1e. Thus, we suggest employing the scatterplot for dispersion analysis.

3.2. *Dipole acoustic logging*

In figures 2 and 3, we present the results for the dipole acoustic logging in a hard and a soft formation, respectively. Figures 2a and 3a are the full waveforms in the time domain, while figure 2b–2f and figure 3b–3d are the corresponding slowness-frequency graphs extracted by using different means.

For the case of the hard formation, as shown in figure 2a, the dominated two wave groups are the S-wave and the Flexural (Fl) wave in order of arrival time. In this case, the P-wave is not identified from the time-domain waveform because of its small amplitude. Figure 2b gives the slowness-frequency snapshot in which all the seven setting modes are involved. Although the S-wave and several orders of the Fl wave as well as the P-wave have been observed, there are serious interferences of the false modes to these true modes. By comparison, the modes in figure 2c are significantly more coherent and smoother than in figure 2b, where the false modes have been removed and four dominated modes have been remained. The comparison result indicates that the scheme of removing false modes proposed in subsection 2.2 works well.

Figure 2d shows the result by WSS. Obviously, the Fl waves of each order only just appear within the 3–10, 10–20 and after 20 kHz, respectively, which indicates the limitation of WSS method that only identifies the strongest mode in each frequency. Shown in figure 2e is the slowness-frequency snapshot after optimising, where the wave groups are more distinctive than in figure 2c. Figure 2f shows the comparison of the slowness scatterplot among the WSS, the modified MP and forward synthetic algorithm. It can be seen that the dispersion data obtained by modified MP algorithm are more comprehensive, including the P- and S- wave that cannot be obtained by the WSS method. Besides, the scatterplot has higher resolution and intuitively shows dispersion characteristics.

From the time-domain waveforms of the soft formation case in figure 3a, it is evident that there are two wave groups in order of arrival time, which are the leaky P wave and the Fl wave. The S-wave is covered by the Fl wave and thus cannot be recognised from figure 3a. As shown in figure 3b, we obtain the slowness-frequency profiles of the leaky P wave and Fl wave by conventional WSS algorithm.

In contrast, in addition to the two waves obtained in figure 3b, our algorithm in figure 3c also obtained additional shear waves. Nevertheless, the slowness-frequency profile of the S-wave is not very clear in figure 3c because of the poor resolution of the snapshot. When we extract the slowness extremum and show it in figure 3d, it is clear that the Fl wave and S-wave are separated intuitively. It illustrates the advantages of the extreme-point extraction scheme proposed in subsection 2.4.

Besides, for both figure 2f and figure 3d, the results of modified MP and forward synthetic algorithm always coincide well, which proves the applicability of modified MP algorithm in dipole acoustic logging.

3.3. *Acoustic LWD*

Acoustic LWD, which acquires formation information in real time, has grown in popularity in recent years (Wang *et al.* 2015). In this subsection, the proposed algorithm is used for acoustic LWD in order to exemplify its performance to process complex signals. At the same time, we discuss the anti-noise ability of this algorithm by processing a noisy signal with a signal-to-noise ratio (SNR) of 10. Figure 4a is the time-domain full waveforms of acoustic LWD, where the dominated waves in order of arrival time are the second order (M2) and first order (M1) drill collar waves, the S and PR wave, the St wave and Inner-Stoneley (In-St). Compared with the wireline logging in subsection 3.1 and 3.2, there are additional wave groups in the LWD waveforms. Besides, some of the waves are overlapped together in time domain and meanwhile their dispersion curves are especially close in the frequency domain, thus the signals of LWD are more complex than those of wireline logging.

In figure 4b, without removing the false modes, we obtain the slowness-frequency graph involving all the eight presetting modes. Obviously, the true modes in figure 4b are seriously disturbed, resulting in difficulties in observation and extraction of dispersion characteristics. Figure 4c shows the snapshot of slowness dispersion involving the five true modes, in which the three false modes have been removed. By comparison, the dispersion characteristics of the true modes are clearly displayed in

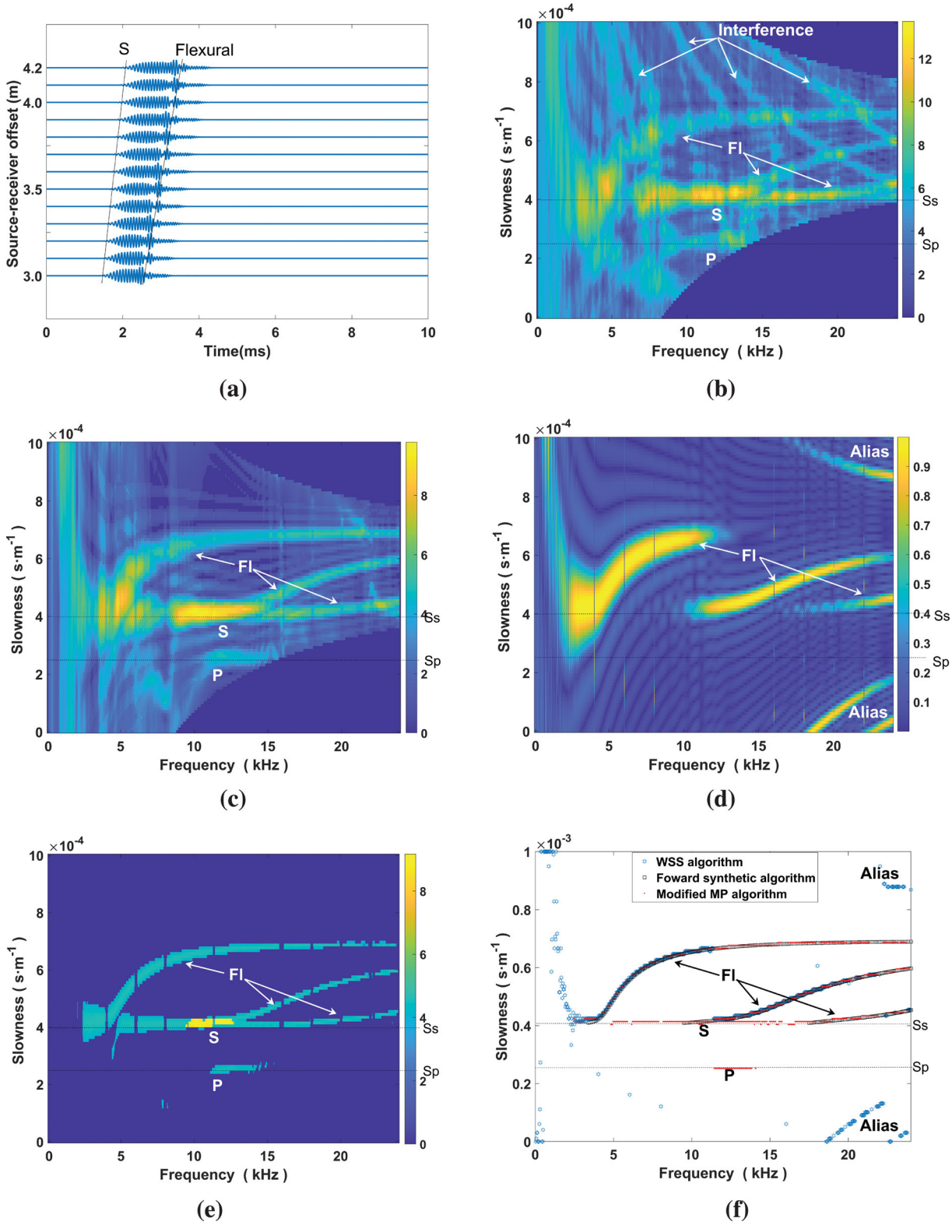

Figure 2. Dipole logging in the hard formation: (a) synthetic time-domain full waveforms; (b) slowness-frequency snapshot involved all the mode waves; (c) slowness-frequency snapshot with removing false modes; (d) slowness-frequency snapshot inverted by the WSS algorithm; (e) slowness-frequency snapshot inverted by the modified MP algorithm proposed in this study and (f) comparison of dispersion scatterplot of WSS algorithm, modified MP algorithm and forward synthetic algorithm.

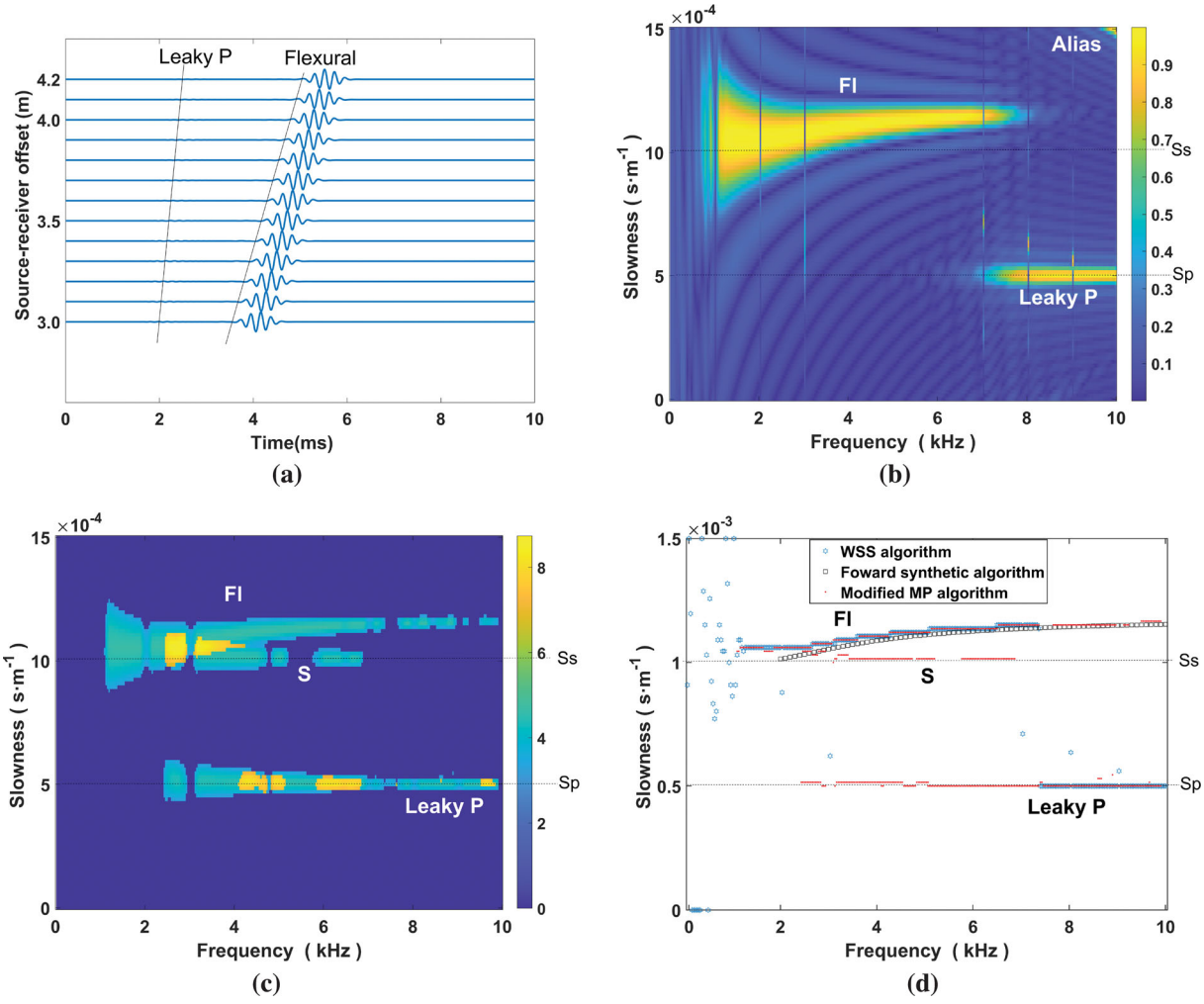

Figure 3. Dipole logging in a soft formation: (a) synthetic time-domain full waveforms; (b) slowness-frequency snapshot inverted by the WSS algorithm; (c) slowness-frequency snapshot inverted by the modified MP algorithm proposed in this study and (d) comparison of dispersion scatterplot of WSS algorithm, modified MP algorithm and forward synthetic algorithm.

figure 4c, without any interference from the false modes, which demonstrates the ability of the proposed algorithm to process complex signals.

Figure 4d compares the dispersion results obtained by different algorithms in the form of a scatterplot. The red points are acquired by extracting the extremum from figure 4c, while the black squares denote forward synthetic results. It is clear that all the extracted dispersion data are identical with the forward calculations, which indicates the correctness of the modified MP algorithm proposed in this paper. Besides, it is worth noting that the In-St wave is extracted successfully by the modified MP algorithm, although the velocity is almost the same as that of the St wave and the amplitude is smaller than that of the St wave. Additionally, similar to figure 1f, the extracted data of the St wave deviates from the forward result at extremely low frequencies.

Figure 4e compares the waveforms of the noiseless signal (the waveform above) and the noisy signal (the waveform below) in the LWD. For the noisy signal, we added white Gaussian noise into the original signal with SNR = 10. It is evident the original signal is subject to serious noise interference that we cannot identify the wave groups of small amplitude such as M1 and M2 drill collar waves. Figure 4f shows a slowness-frequency inversion snapshot of noisy signal. The result shows that almost all mode waves still can be clearly identified except the In-St wave, which is submerged by noise. In fact, two steps in our algorithm can remove the noise, the first uses forward and backward MP average calculation (Ekstrom 1996), the second is the proposed scheme for removing false modes in subsection 2.2. Despite this, some wave groups with low energy will be covered by the introduced noise, which therefore is hard to recover. However, the wave groups with high energy are almost unaffected by the noise.

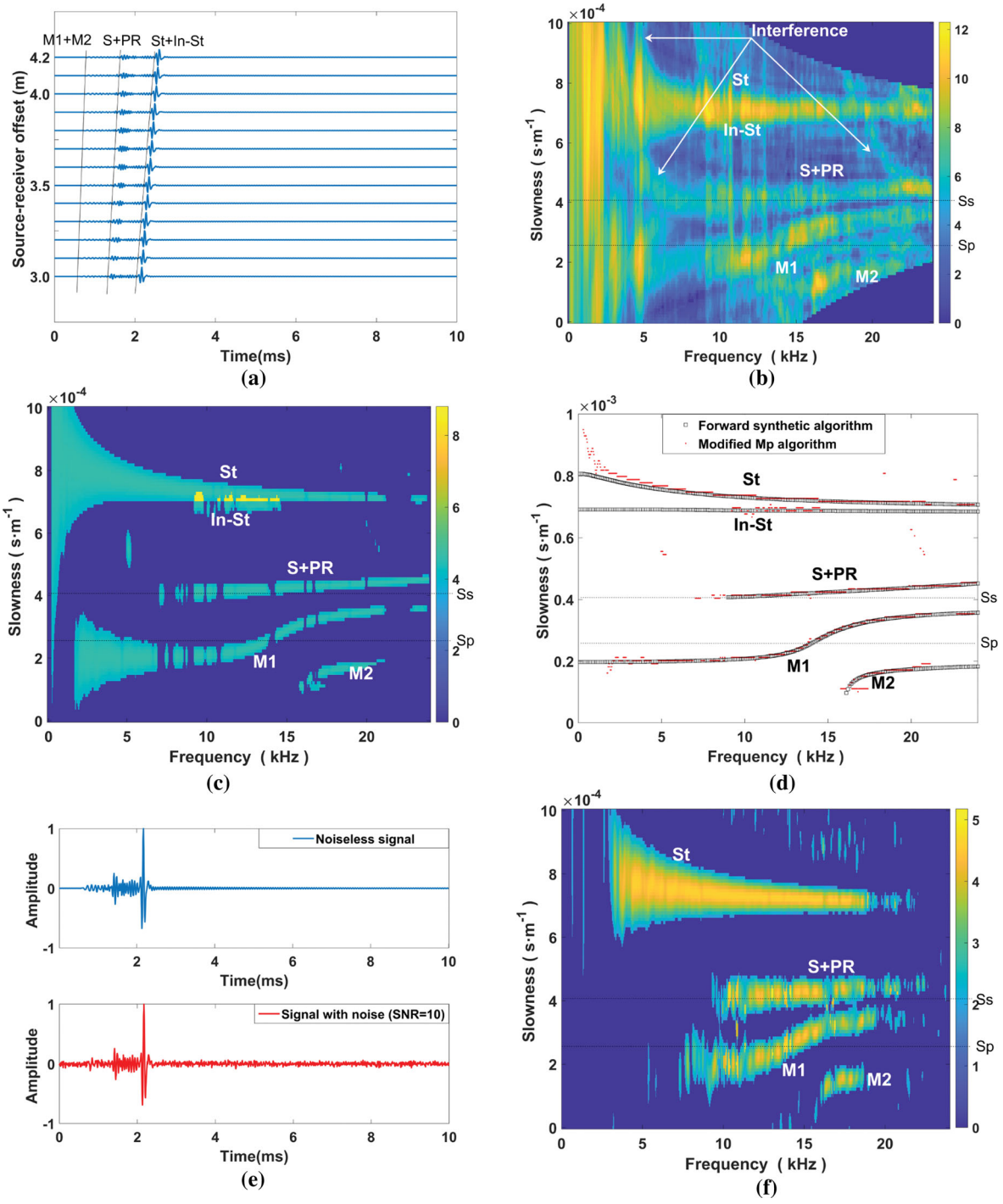

Figure 4. Acoustic logging while drilling in a hard formation: (a) synthetic time-domain full waveforms; (b) slowness-frequency snapshot involving all the mode waves; (c) slowness-frequency snapshot with removing false modes; (d) comparison of dispersion scatterplot of WSS algorithm, modified MP algorithm and forward synthetic algorithm; (e) comparison of noiseless signal and noisy signal (SNR = 10) and (f) slowness-frequency inversion snapshot of noisy signal.

4. Conclusions

We have improved the mode-wave inversion combining MP and WSS algorithms. In terms of the four synthetic cases of acoustic logging, it has been demonstrated that the proposed modified MP algorithm performs better than previous ones in slowness resolution and display definition. Even for the acoustic LWD with complex wave components, it extracts accurate dispersion characteristics of all the mode waves as well as the P- and S-waves.

The innovations and advantages of the proposed algorithm are summarised as follows: (1) by introducing a threshold of the energy spectrum, we have successfully removed all the false modes and thus eliminated their interference to the true modes. In slowness-frequency graphs, the dispersion profiles of the mode waves are coherent and smooth. (2) By setting an optimised coefficient to reject smaller semblance coefficients of slowness-frequency snapshot, we have contributed to the acquisition of dominated wave groups and meanwhile excluded dispersion points outside the cut-off frequency. It shows the pre-optimisation scheme is helpful to reflect the dispersion characteristics accurately. (3) By an ingenious means, superimposing the extremum extracted from the slowness-frequency snapshot of every single-mode, we obtain a scatterplot with a higher slowness-resolution than the snapshot. It is demonstrated that the proposed algorithm performs well at distinguishing two mode waves with similar velocities (the dispersion curves are close to each other). (4) By processing a signal containing noise (SNR = 10) in the LWD, the good anti-noise ability of the proposed algorithm is shown.

Acknowledgements

This work is jointly supported by National Natural Science Foundations of China (grant nos. 41874129, 41574112 and 11734017) and the National Science and Technology Major Project of China (grant no. 2017ZX05019006–006).

Conflict of interest statement. None declared.

References

Ekstrom, M.P., 1996. Dispersion estimation from borehole acoustic arrays using a modified matrix pencil algorithm, *IEEE Conference Record of the Twenty-Ninth Asilomar Conference on Signals, Systems and Computers*, **1**, 449–453.

Hua, Y. & Sarkar, T.K., 1990. Matrix pencil method for estimating parameters of exponentially damped/undamped sinusoids in noise, *IEEE Transactions on Acoustics, Speech, and Signal Processing*, **38**, 814–824.

Jiang, C., Tang, X.M., Su, Y.D., Zhuang, C.X. & Lee, S.Q., 2017. Compressional and shear slowness processing by joint inversion of multipole acoustic-array data, *SEG Technical Program Expanded Abstracts*, pp. 844–848.

Kimball, C.V. & Marzetta, T.L., 1984. Semblance processing of borehole acoustic array data, *Geophysics*, **49**, 274–281.

Li, J. & Stoica, P., 1996. An adaptive filtering approach to spectral estimation and SAR imaging, *IEEE Transactions on Signal Processing*, **44**, 1469–1484.

Li, W., Tao, G., Matuszyk, P.J. & Torres-Verdín, J., 2015. Forward and backward amplitude and phase estimation method for dispersion analysis of borehole sonic measurements. Borehole dispersion analysis with FBAPES, *Geophysics*, **80**, D295–D308.

Lang, S.W., Kurkjian, A.L., McClellan, J.H., Morris, C.F. & Parks, P.W., 1987. Estimating slowness dispersion from arrays of sonic logging waveforms, *Geophysics*, **52**, 530–544.

Ma, J., Matuszyk, P.J., Mallan, R.K., Torres-Verdín, C. & Voss, B.C., 2010. Joint processing of forward and backward extended Prony and weighted spectral semblance methods for robust extraction of velocity dispersion data, *SPWLA 51st Annual Logging Symposium*, SPWLA-2010-34072.

Nolte, B., Rao, R. & Huang, X., 1997. Dispersion analysis of split flexural waves, Massachusetts Institute of Technology, *Earth Resources Laboratory*.

Penrose, R., 1955. A generalized inverse for matrices, *Mathematical Proceedings of the Cambridge Philosophical Society*, **51**, 406–413.

Plona, T.J., Kane, M.R., Sinha, B. & Wash, J., 2002. Evaluating stress-induced anisotropy and mechanical damage from cross-dipole sonic data using dispersion analysis, *Rock Mechanics Conference, Society of Petroleum Engineers*.

Sinha, B.K., Kane, M.R. & Frignet, B., 2000. Dipole dispersion crossover and sonic logs in a limestone reservoir, *Geophysics*, **65**, 390–407.

Sinha, B.K., Norris, A.N. & Chang, S.K., 1994. Borehole flexural modes in anisotropic formations, *Geophysics*, **59**, 1037–1052.

Su, Y.D. & Qiao, W.X., 2003. A method to extract phase slowness of dispersive wave from sonic logging data, *Well Logging Technology*, **27**, 364–368 (in Chinese).

Tamarkin, J., 1926. A new proof of Parseval's identity for trigonometric functions, *Annals of Mathematics*, 541–547.

Tang, X.M., 1997. Predictive processing of array acoustic waveform data, *Geophysics*, **62**, 1710–1714.

Tang, X.M. & Cheng, C.H., 2004. *Quantitative Borehole Acoustic Methods*, Petroleum Industry Press: Beijing.

Tang, X.M., Reiter, E.C. & Burns, D.R., 1995. A dispersive-wave processing technique for estimating formation shear velocity from dipole and Stoneley waveforms, *Geophysics*, **60**, 19–28.

Tribolet, J., 1977. A new phase unwrapping algorithm, *IEEE Transactions on Acoustics, Speech, and Signal Processing*, **25**, 170–177.

Tsang, L. & Rader, D., 1979. Numerical evaluation of the transient acoustic waveform due to a point source in a fluid-filled borehole, *Geophysics*, **44**, 1706–1720.

Wang, H., Tao, G. & Fehler, M., 2015. Investigation of the high-frequency wavefield of an off-center monopole acoustic logging-while-drilling tool, *Geophysics*, **80**, D329–D341.

Wang, R.J., Qiao, W.X. & Ju, X.D., 2012. A multi-channel acoustic logging signal dispersion analysis method, *Well Logging Technology*, **36**, 135–140 (in Chinese).

Xu, S., Tang, X.M., Su, Y.D., Lee, S.Q. & Zhuang, C.X., 2017. Determining formation S-wave transverse isotropy from borehole flexural-wave dispersion data, *Geophysics*, **82**, D47–D55.

Zeng, F.Q., Yue, W.Z. & Li, C., 2018. Dispersion analysis of borehole sonic measurements by Hilbert transform and band-pass filters, *Geophysics*, **83**, D127–D150.

Zhao, X. & Ye, B., 2011. Selection of effective singular values using difference spectrum and its application to fault diagnosis of headstock, *Mechanical Systems and Signal Processing*, **25**, 1617–1631.

Zheng, X.B., Hu, H.S., Guan, W. & Wang, J., 2015. Simulation of the borehole quasistatic electric field excited by the acoustic wave during logging while drilling due to electrokinetic effect, *Geophysics*, **80**, D417–D427.